Supplementary Information

Direct Laser Writing of Four-Dimensional Structural Color Microactuators Using a Photonic Photoresist

Marc del Pozo [1], Colm Delaney [2], Cees W.M. Bastiaansen [1,3], Dermot Diamond [4],

*Albert P.H.J. Schenning [1] * and Larisa Florea [2] ***

[1] Stimuli-responsive Functional Materials and Devices, Department of Chemical Engineering, Eindhoven University of Technology, P.O. Box 513, 5600 MB Eindhoven, The Netherlands.

[2] School of Chemistry and AMBER, the SFI Research Centre for Advanced Materials and BioEngineering Research, Trinity College Dublin, the University of Dublin, College Green, Dublin 2, Ireland.

[3] School of Engineering and Materials Science, Queen Mary University of London, Mile End Road, London E1 4NS, UK.

[4] Insight Centre for Data Analytics, National Centre for Sensor Research, School of Chemical Sciences, Dublin City University, Glasnevin, Dublin 9, Ireland.

* Corresponding author´s e-mail: a.p.h.j.schenning@tue.nl and floreal@tcd.ie

Methods

   Coating Preparation. A glass slide was functionalized with methacrylate groups by first treating it in a UV-ozone photoreactor (Ultra Violet Products, PR-100) for 20 min. The surface of the activated glasses was then functionalized by spin coating (3000 rpm, 45 s) a 3-(trimethoxysilyl)propyl methacrylate solution (1 vol. % solution in a 1:1 water-isopropanol mixture) followed by a curing step of 10 min at 100 °C. The cholesteric liquid crystalline (CLC) mixture was applied on top of the functionalized glass and a clean glass substrate placed on top. The two glasses were sheared along one direction to obtain alignment. Photo-copolymerization of the monomer mixture was performed at room temperature with an Exfo Omnicure S2000 light source in which 57% of the light intensity has a wavelength of 395-445 nm and 43% of 320-390 nm.

   Differential Scanning Calorimetry. Differential scanning calorimetry (DSC) was performed with a DSC Q2000 from TA Instruments with an aluminum hermetic crucible. All tests were conducted in nitrogen environment. The temperature range was between -20 °C and 100 °C with heating and cooling rates of 5 °C/min. Three cycles were performed per measurement.

   UV-Visible Spectroscopy. A Perkin Elmer Lambda 750 spectrometer equipped with a 150 mm integrating sphere, with a tungsten halogen light source was used to measure the reflection spectra of a coating made from the photonic-photoresist between 300 and 800 nm.

   Raman Spectroscopy. Raman spectra were recorded on a Bruker SENTERRA dispersive Raman microscope. A confocal line scan was measured at the center of the structure and to a drop of the photonic-photoresist using a 785 nm laser, 100x objective with a 3 min integration time per measurement.

Characterization of the photoresist

The phase and stability of the CLC phase of the photoresist were studied *via* DSC measurements (**Figure S1**). The traces from the heating and cooling cycles show a phase transition around 50 °C, which corresponds to transitions from isotropic to chiral nematic, as confirmed by crossed polarized micrographs. The stability of the phase at room temperature was analyzed by performing an isothermal measurement at 20 °C for 8 hours. No peak was observed indicating that no phase transition occurred during this period indicating a stable liquid crystalline phase at 20 °C for at least 8 hours. Finally, the position of the reflection band was measured for a coating at 400 nm (**Figure S2**). Then the coating was treated for 10 min with a solution of 1M KOH aq. to cleave the hydrogen bonds and form a photonic polymer salt. The reflection spectrum was measured again showing a less intense peak than before the base treatment at the same position. The lower intensity of the peak is attributed to the increase of molecular disorder due to the cleavage of the hydrogen bonds.[1]
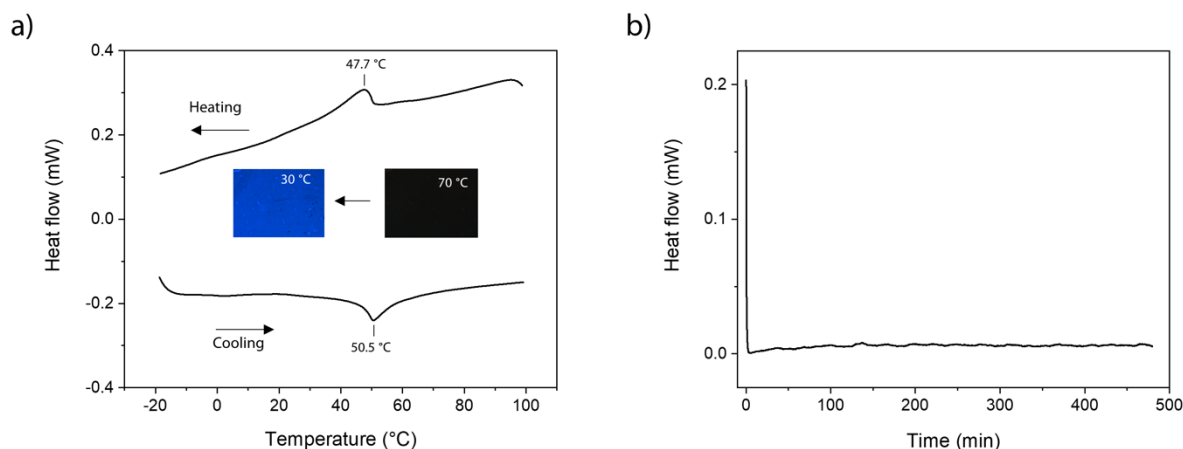

Figure S1. DSC measurements of the photonic-photoresist; a) DSC traces of heating and cooling cycles. Inset: crossed polarized micrographs taken at 60 °C, showing mixture in the isotropic phase, and at 30 °C, showing mixture in the chiral nematic phase; b) Isothermal measurement after cooling from 100 °C to 20 °C, at 20 °C over 8 h.
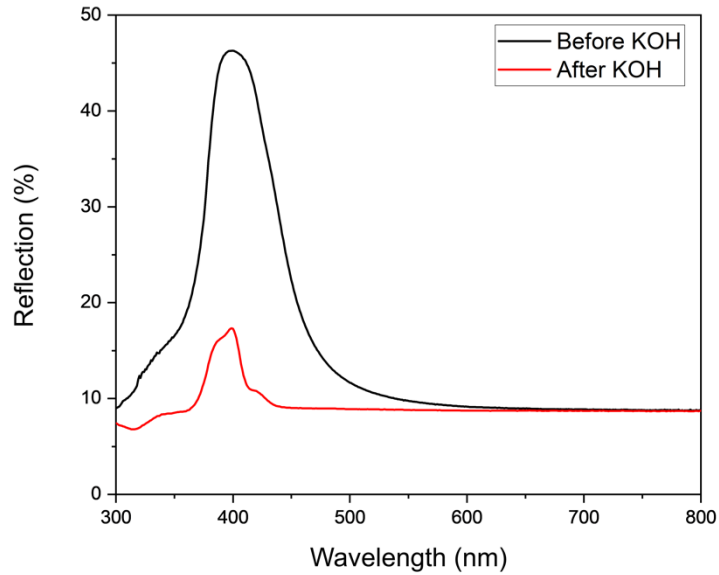
Figure S2. UV-Visible spectrum of a coating made from the photonic-photoresist. Black trace shows the coating before base treatment; red trace shows measurement after base treatment (immersion of the coating in a 1M KOH aq. solution for 10 min).
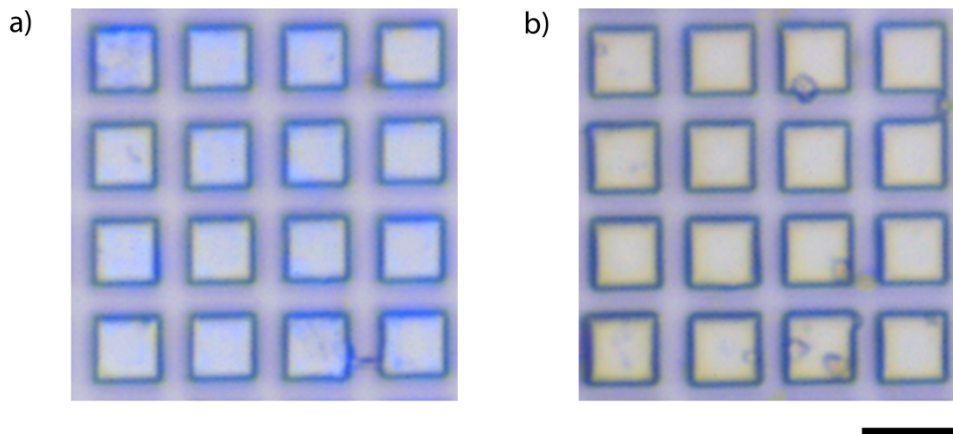
Arrangement of pillars

Figure S3. Light micrographs of an arrangement of pillars before (a) and after (b) activation. The scale bar represents 10 μm.

Cross polarization to enhance visualization of the microstructures' optical properties

Due to the small dimensions of the structures, the structural color can be challenging to appreciate at high magnifications as less light reaches them and therefore less light is reflected by them. Furthermore, the light reflected by the glass substrate masks the reflected light by the structures. In order to remove the light contribution of the glass and to only observe the light reflected by the CLC, the structures were placed between crossed linear polarizers (**Figure S4**). This effect is caused by the ability of CLCs to change the polarization of the light. This occurs because linearly polarized light can be described as a composition of an equal amount (50 %) of left- and right-handed circularly polarized light. Therefore, linear polarized light can be expressed in the following way when using Jones vectors: $[1\ 0] = 1/\sqrt{2}\ [1\ i] + 1/\sqrt{2}\ [1-i]$. Thus 50 % of the linear polarized light in the reflection band of the CLC is reflected as right-handed circularly polarized light and can go through the analyzer. This does not occur with the light that is reflected by the glass substrate. As a result, when observing the structures between crossed linear polarizers only the light reflected by the CLC structures is detected.
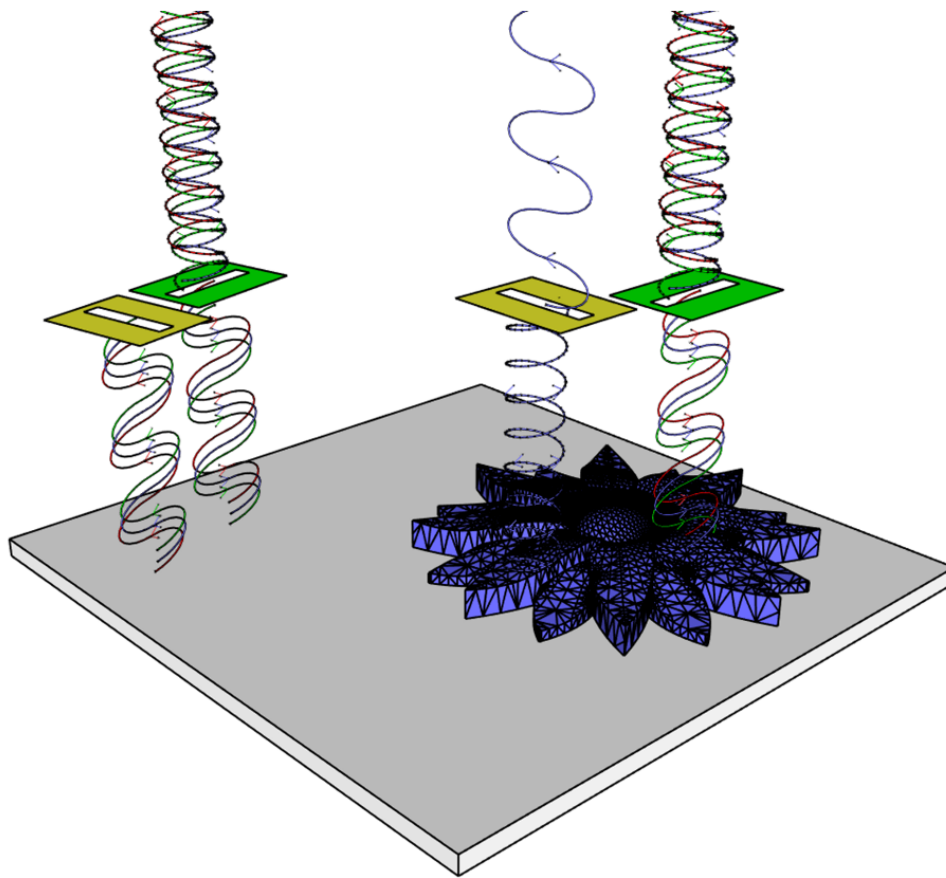
Figure S4. Image depicting the difference between the polarization of the light reflected by the structures and by the glass. The polarizer represented in green serves to filter the indicent light and the polarizer represented in yellow, filters the refected light. As the glass substrate does not change light's polarization, the reflected light by the glass is removed, thereby allowing light reflected by the structure to pass through the polarizer.

Confocal Raman Spectroscopy

The verification of successful two photon-polymerization (TPP) and cleavage of the hydrogen bonds during the activation step (Step 2) was conducted by confocal Raman spectroscopy analysis of the photonic-photoresist and microstructures (**Figure S5**). After printing, the peak at 1635 cm^{-1}, corresponding to the stretch of the C=C bond in the acrylate groups is reduced, indicating succesful polymerization of the monomer mixture. After the activation step, a reduction in the shoulders at 1647 cm^{-1} and at 1280 cm^{-1} corresponding to C=O and C-O bond stretches, from the carboxylic acid, indicates cleavage of the hydrogen bonds. The appearance of a strong peak at 1395 cm^{-1}, corresponding to the symmetric streatching of CO_2^- from the carboxylic salt, indicates the formation of the polymer salt after the activation step.
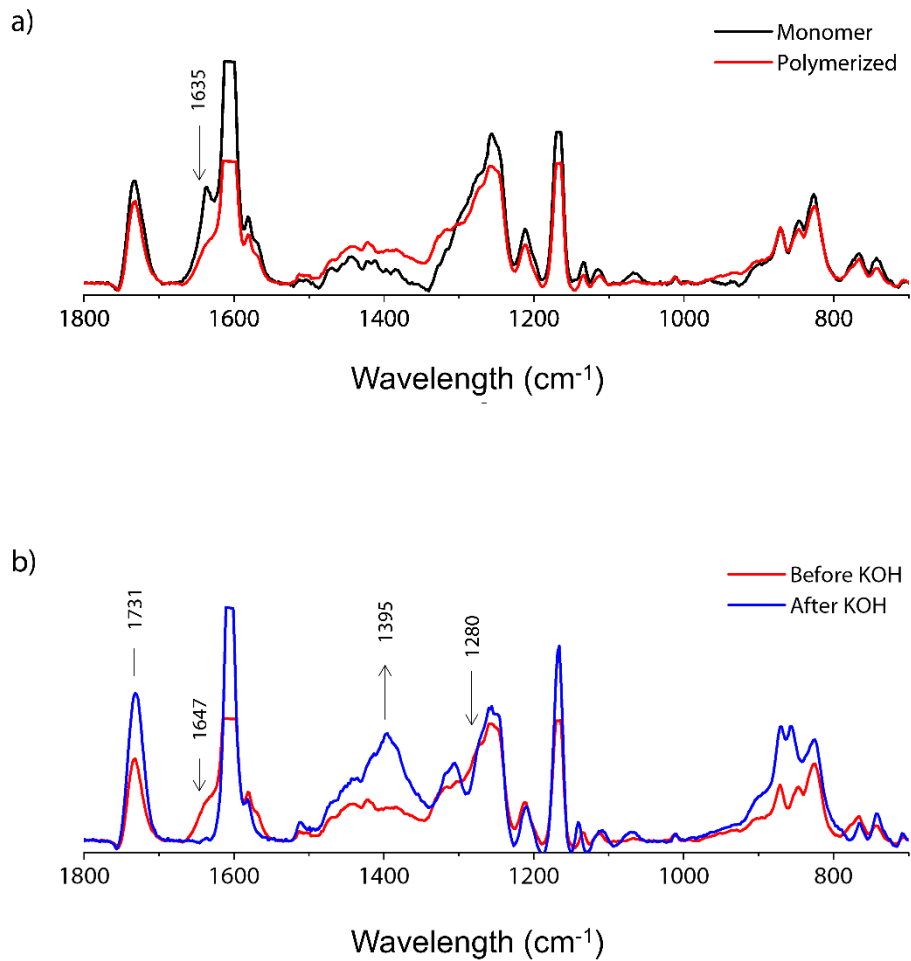
Figure S5. Cofocal Raman spectroscopy showing a) spectra of the unpolymerised photonic-photoresist (i.e monomer), and the polymerized microstructure obtained *via* TPP. b) spectra of obtained microstructures before (red) and after base treatment (blue). All spectra were normallized to the C≡N bond at 2200 cm^{-1}.

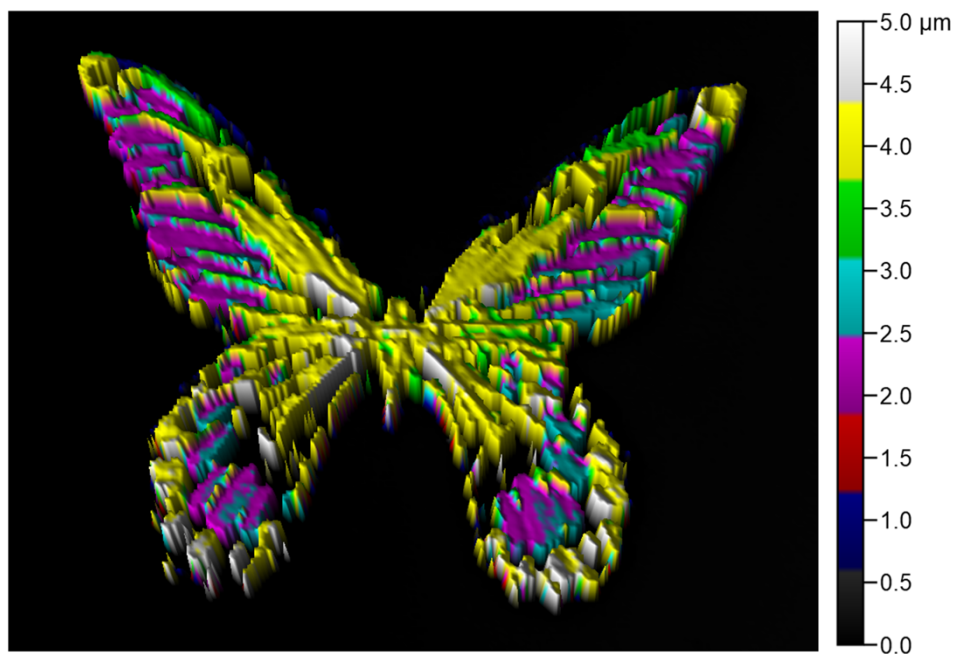**Complementary characterization of micron-sized structures**

Figure S6. 3D profile of the butterfly obtained *via* an optical profiling system.
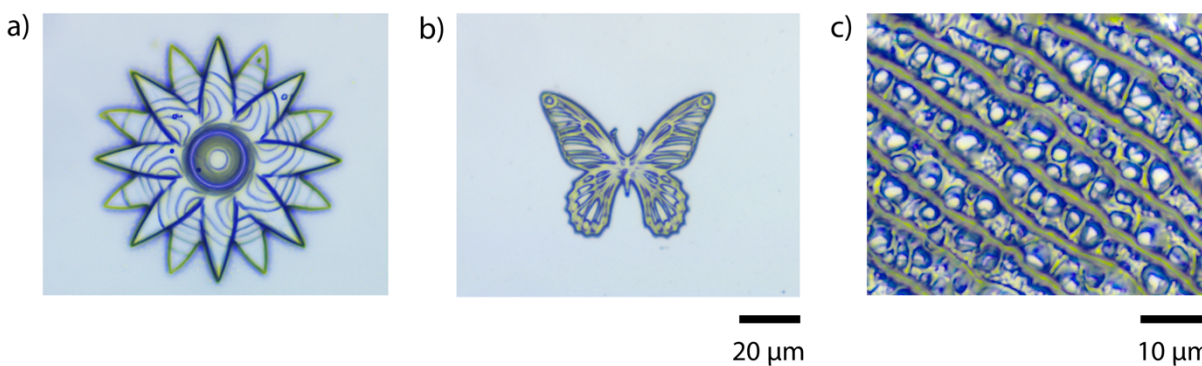

Figure S7. 3D photonic microstructures after base treatment; a) flower, b) butterfly, and c) nanostructured biomimetic pattern.

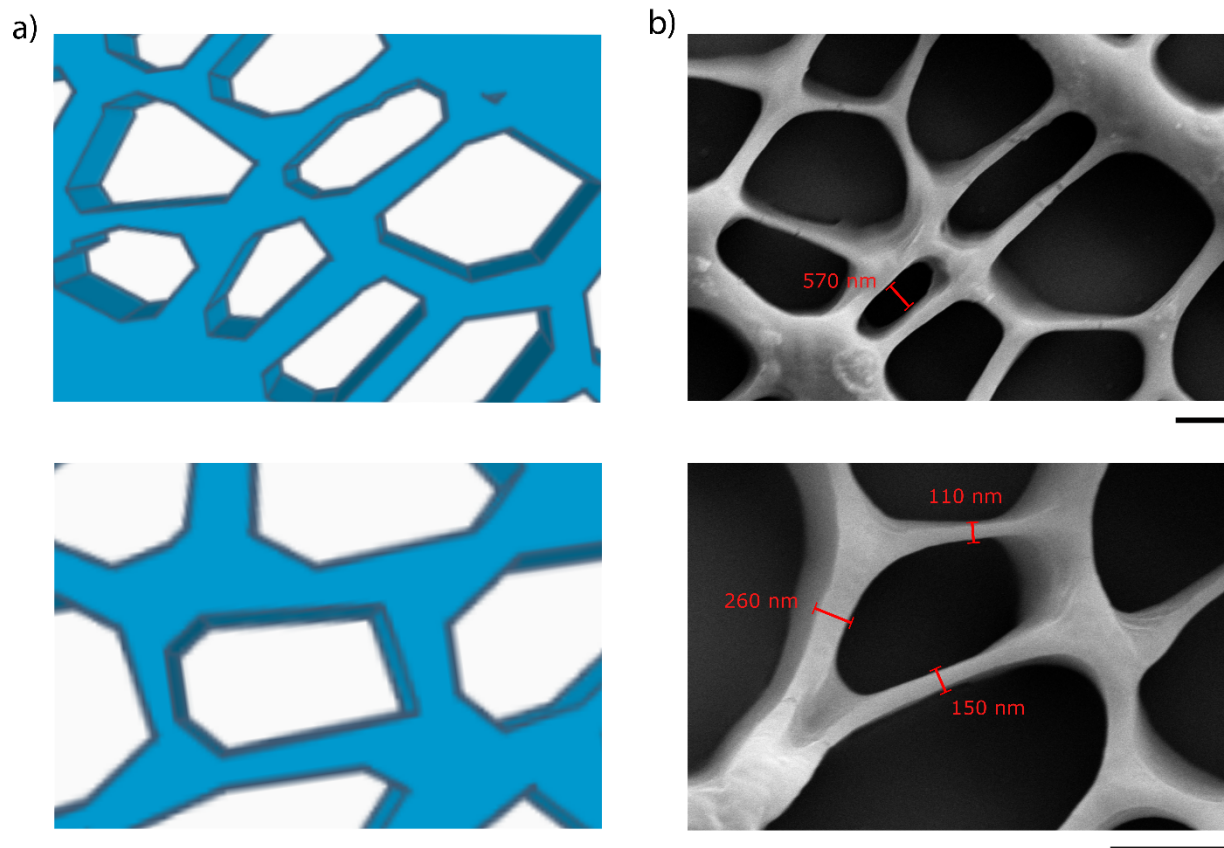**Printing sub-micron features**

Figure S8. Zoom-in from the pattern of the wing of the *Papilio paris* butterfly before base treatment; a) CAD design; b) Scanning electron microscopy (SEM) images. Scale bars represent 1 μm.
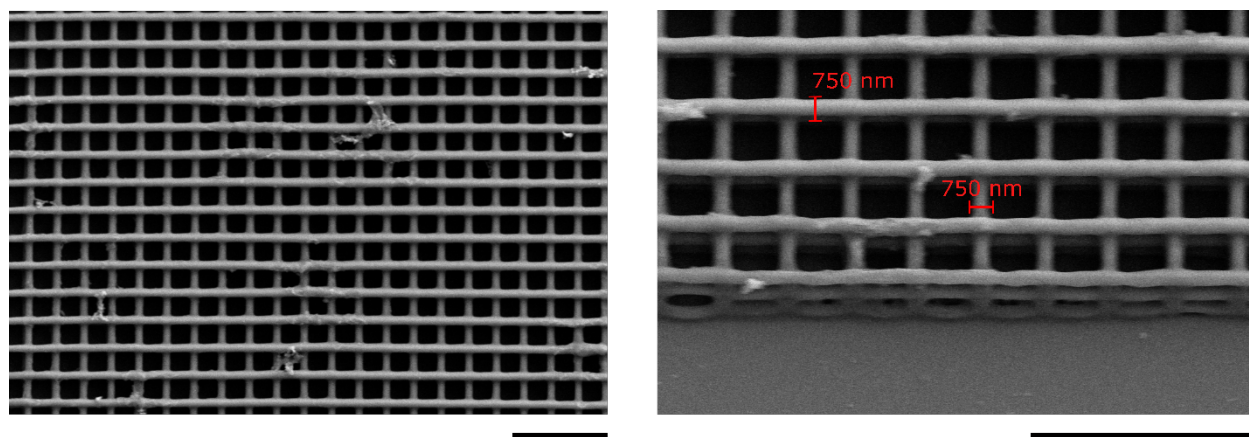

Figure S9. SEM images showing a woodpile structure (before base treatment) fabricated by successive stacking of 750 nm lines rotated orthogonally. Scale bars represent 10 μm.
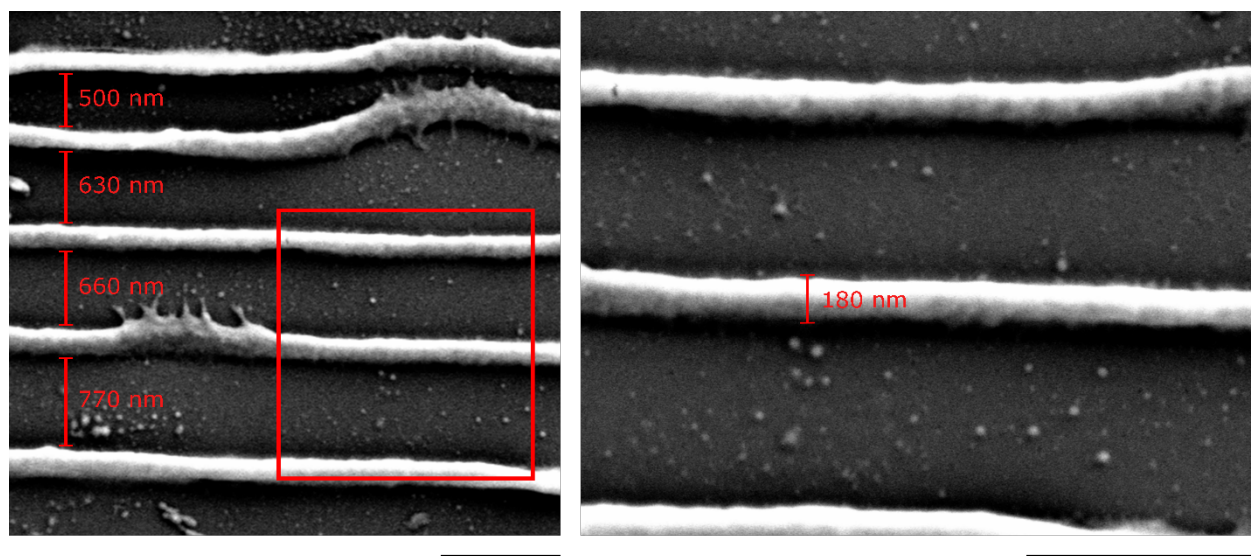
Figure S10. SEM images of an array of lines comprising a single voxel in width and height. Scale bars represent 1 μm.

Influence of structure height on intensity of observed color

As observed across the structures presented herein, the structure dimensions and geometry greatly impact the observed reflected color. This is attributed to a minimum feature thickness (and pitch) required to efficiently reflect light, as observed in **Figure S11**.
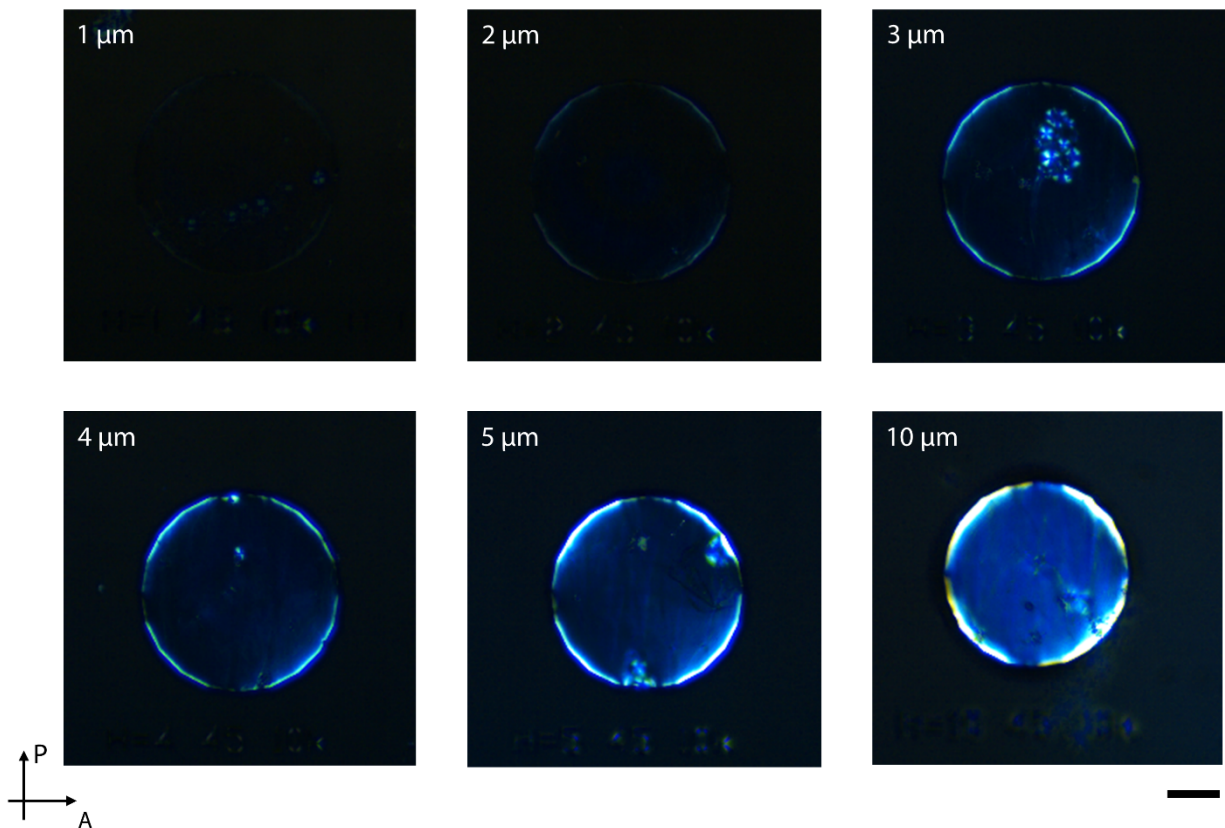

Figure S11. Varying heights of a circular pillar demonstrating the effect on reflected structural color of the structures. All images were taken using the same camera acquisition settings. The scale bar represents 20 μm.

Dew point calculation

The extended Magnus equation, **Equation S1**, gives the relationship between the dew point and the relative humidity and temperature.[2] In the equation, T_d is the temperature of the dew point (°C), RH is the relative humidity (%) and T is the temperature (°C). The values of the coefficient A and B are obtained from literature, A= 17.625 °C and B =243.04 °C.[3]

$$T_d = \frac{B * \left(ln \left(\frac{RH}{100} \right) + \frac{A \cdot T}{B + T} \right)}{A - ln \left(\frac{RH}{100} \right) + \frac{A \cdot T}{B + T}} \tag{1}$$
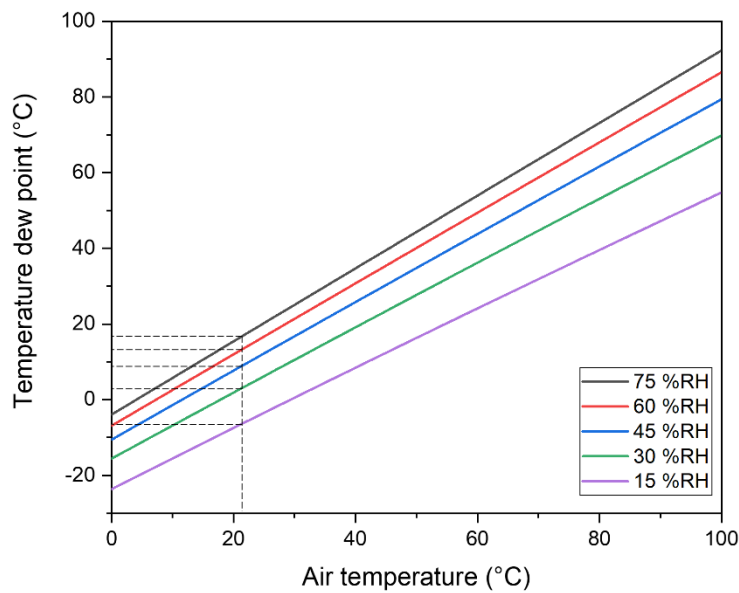

Figure S12. Representation of the relationship between the dew point and the air temperature. The data point were calculated using **Equation S1**. The dashed line shows the different position of the different dew point at an air temperature of 23 °C which correspond to 18 °C, 15 °C, 10 °C, 5 °C and -5 °C for 75 %RH, 60 %RH, 30 %RH and 15 %RH respectively.

Optical response of a microflower by varying temperature at constant humidity
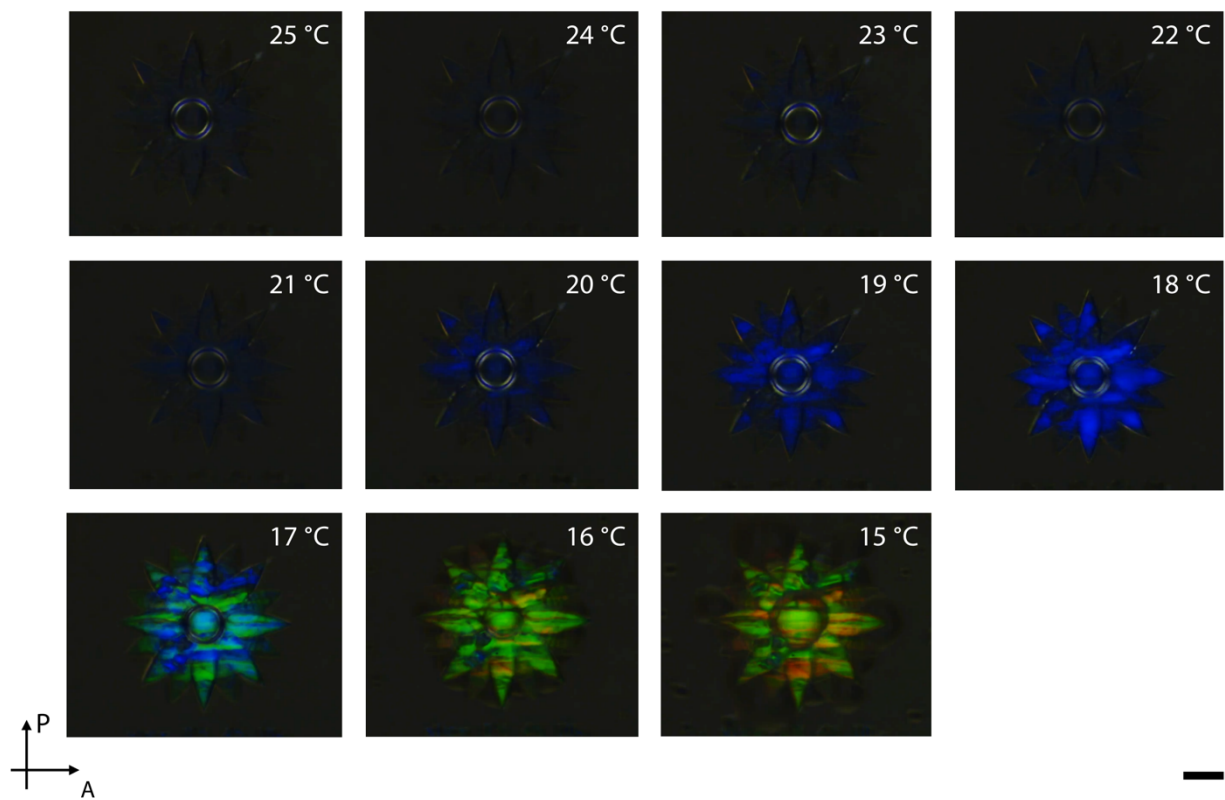

Figure S13. Crossed polarized micrographs of a micron sized flower at varying temperatures with constant humidity (75 %RH). The scale bar represents 20 μm.

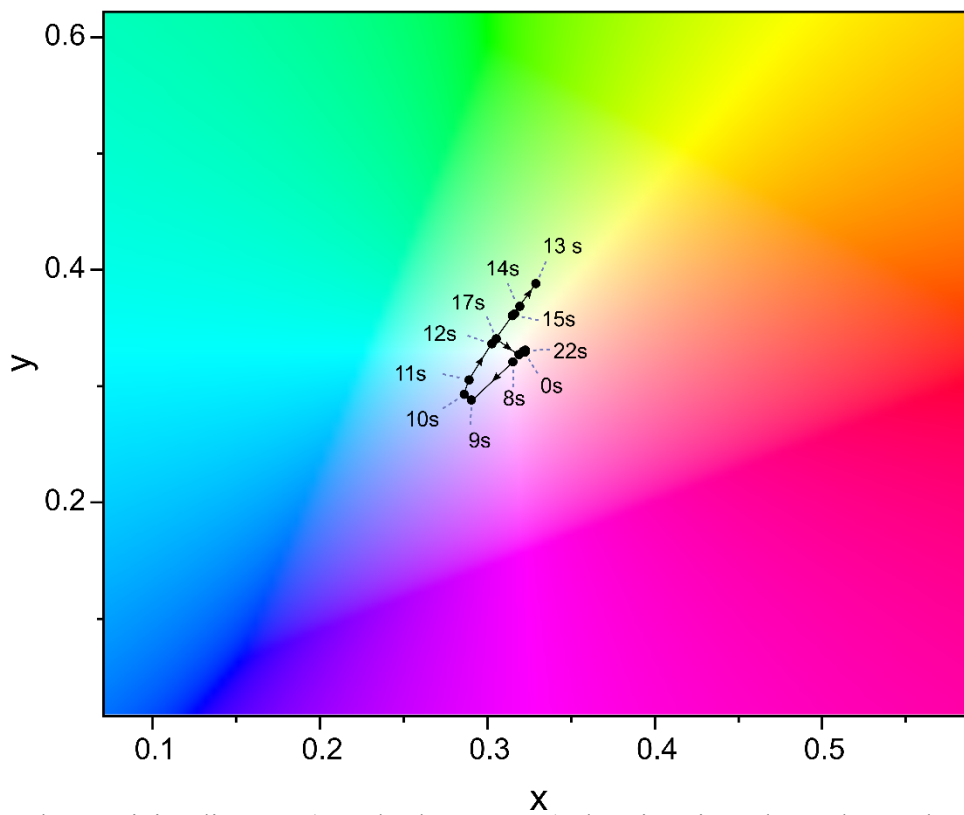**Time-dependent color change of the microflower with changing humidity**

Figure S14. Chromaticity diagram (standard CIE 1931) showing time-dependent color changes of the flower in response to human breath. The data is obtained after analyzing the frames from **Video V1**.

Calculating specific humidity from a relative humidity value

The percentage of relative humidity (%RH) is defined at a given air temperature as the ratio of the partial water vapor pressure (e) to the saturation vapor pressure (e_s) as follow:

$$\%RH = \frac{e}{e_s(T)} \cdot 100 \tag{2}$$

The saturation vapor pressure is temperature dependent and can be expressed using the proposed equation by Murray, **Equation 3**, in which T is the temperature of the air, in Kelvin, and the constants have a value of $a = 17.2693882$ and $b = 35.86$.[4]

$$e_s(T) = 6.1078 \cdot \exp\left(\frac{a\,(T - 273.16)}{T - b}\right) \tag{3}$$

On the other hand, the specific humidity (q) is defined as the mass of water vapor in a unit mass of moist air and can be calculated using the following equation:

$$q = \frac{\frac{M_{water}}{M_{air\,dry}} \cdot e}{p - \left(1 - \frac{M_{water}}{M_{air\,dry}}\right) \cdot e} = \frac{0.622 \cdot e}{p - 0.378 \cdot e} \tag{4}$$

Using **Equations 2-4** we can derive **Equation 5** and calculate the specific humidity from a relative humidity value at a given temperature as shown in **Table S1**.

$$q = \frac{0.03799 \cdot \%RH \cdot \exp\left(\frac{a\,(T - 273.16)}{T - b}\right)}{p - 0.02308 \cdot \%RH \cdot \exp\left(\frac{a\,(T - 273.16)}{T - b}\right)} \tag{5}$$

Table S1. Relative humidity with respect to the specific humidity value for different substrate temperatures.

Temperature of substrate (K)	Air temperature (K)	Relative humidity (%)	Specific humidity (Kg/Kg)
≥ 303.15	296.15	15	0.0263
		30	0.0534
		45	0.0814
		60	0.1103
		75	0.1403
323.15	297.15	15	0.0279
		30	0.0568
		45	0.0867
		60	0.1177
		75	0.1498
343.15	299.15	15	0.0315
		30	0.0643
		45	0.0983
		60	0.1338
		75	0.1707

References

(1)   van Kuringen, H. P. C.; Leijten, Z. J. W. A.; Gelebart, A. H.; Mulder, D. J.; Portale, G.; Broer, D. J.; Schenning, A. P. H. J. Photoresponsive Nanoporous Smectic Liquid Crystalline Polymer Networks: Changing the Number of Binding Sites and Pore Dimensions in Polymer Adsorbents by Light. *Macromolecules.* **2015**, *48*, 4073–4080.

(2)   Lawrence, M. G. The Relationship between Relative Humidity and the Dewpoint Temperature in Moist Air: A Simple Conversion and Applications. *Bull. Am. Meteorol. Soc.* **2005**, *86*, 225–233.

(3)   Alduchov, O. A.; Eskridge, R. E. Improved Magnus Form Approximation of Saturation Vapor Pressure. *J. Appl. Meteorol.* **1996**, *35*, 601–609.

(4)   Murray, F. W. On the Computation of Saturation Vapor Pressure. *J. Appl. Meteorol.* **1967**, *6*, 203–204.